The event-to-event variability of the boreal winter MJO

Hugo Bellenger, Jean-Philippe Duvel

The event-to-event variability of the boreal winter MJO

H. Bellenger[1] and J. P. Duvel[2]

Received 15 February 2012; revised 13 March 2012; accepted 14 March 2012; published 20 April 2012.

[1] During boreal winters, perturbations of the convection by the Madden-Julian Oscillation (MJO) peak over three basins distributed in longitude south of the Equator: the eastern Indian Ocean (IO), the south of the Maritime Continent (MC) and the western Pacific Ocean (PO). We use the observed Outgoing Longwave Radiation (OLR) and low-level wind to identify and characterize all wintertime MJO events between 1979 and 2010. There is a large event-to-event variability with some MJO events organized at the planetary-scale having their amplitude well distributed over the 3 basins and some showing only basin-scale organization with a convective perturbation peaking over one or two basins. The average of the MJO amplitude for the three basins shows an intriguing decadal variability consistent for both OLR and low-level wind. The disparity between the 3 basins is dominated by an alternation between MJO amplitude peaking on either the Indian or the Pacific Ocean. This Indo-Pacific alternation, depicted by an Indo-Pacific Index (IPI), is partly related to ENSO. In El Niño conditions, there is not only an extension of the MJO perturbation further east, but also an increase of the MJO perturbation over the western Pacific and a diminution of the MJO perturbation over the eastern Indian Ocean. **Citation:** Bellenger, H., and J. P. Duvel (2012), The event-to-event variability of the boreal winter MJO, *Geophys. Res. Lett.*, *39*, L08701, doi:10.1029/2012GL051294.

1. Introduction

[2] The canonical Madden-Julian Oscillation (MJO) is a planetary-scale (up to 10^4 km) intraseasonal (20–90 days) perturbation of wind and convection that propagates slowly eastward ($\sim$5 m.s^{-1}) near the equator from the Indian Ocean to the Western Pacific Ocean [e.g., *Zhang*, 2005]. Typically, this defines circulation anomalies that travel eastward at a regular speed with convective systems embedded in the ascending branch. However, beside this canonical view, there are relatively strong variations in the planetary-scale patterns of the intraseasonal perturbations. The seasonal cycle modulates the latitudinal position of these perturbations [see *Zhang*, 2005], with a large month-to-month variation of the monthly average patterns, especially within the boreal summer season [*Bellenger and Duvel*, 2007]. There are also known interannual variations of the MJO position with, for example, an eastward extension of the perturbations over the western Pacific Ocean during El Niño events [*Kessler*, 2001]. *Jones et al.* [2004] identified three different types of intraseasonal events, those concentrated over the Indian Ocean and those propagating either eastward (MJO type) or northeastward depending on the season. They found that both Indian Ocean and MJO types occur mostly during Boreal Winter, with no evident relation with ENSO.

[3] Even within a given season, there is a significant event-to-event variability of the planetary-scale pattern (i.e., several oceanic basins) of the perturbations [*Goulet and Duvel*, 2000]. This intermittent nature of the perturbations led some authors to describe MJO as a series of pulse-like events [*Yano et al.*, 2004]. *Duvel and Vialard* [2007] further noticed that, while the planetary-scale perturbation pattern is indeed quite variable, the patterns of wind and precipitation are well reproducible at the basin scale for a given season. This feature is a good basis for GCM evaluations [*Xavier et al.*, 2010; *Duvel et al.*, 2012].

[4] Following *Duvel and Vialard* [2007], the present analysis aims to study how the boreal winter MJO events are distributed over three oceanic basins, namely the eastern Indian Ocean (IO), the south part of the Maritime Continent (MC) and the western Pacific Ocean (PO). In order to better understand the origin of the propagation across the Indo-Pacific area, it is particularly interesting to know if most MJO events tend to be evenly distributed over the three basins or if a significant number of MJO events tend to be confined over only one or two basins. It is also interesting to know how this distribution varies in time. As shown by *Bellenger et al.* [2009], a basin-scale organization of the convection gives a non-linear dynamical response that impacts the average circulation. The longitudinal distribution of the MJO perturbation, for one or several events, will thus impact the seasonal average circulation over the Indo-Pacific region. The knowledge of this amplitude distribution is also a basis for further study of the physical processes responsible for the MJO initiation. For example, a strong MJO perturbation over the West Pacific only, instead of the canonical propagation from the Indian Ocean, could be due either to a reinforcement of the MJO amplitude over this region or to a local initiation due to a basin-scale convective development. These points are critical for MJO forecast. In this study, we first identify each boreal winter MJO event using the observed OLR time series and an original approach that detect and characterize objectively an ensemble of planetary-scale organized intraseasonal perturbations. This approach ensures that the planetary-scale pattern of the considered perturbations corresponds to organized MJO perturbations and not to local red-noise variability. We thus perform different diagnostics in order to characterize the event-to-event variability of the longitudinal distribution of the MJO amplitude. We finally discuss these results.

2. Data and Method

[5] We use the daily mean NOAA OLR on 2.5° regions for the 1979–2010 period as a proxy for tropical deep

[1]Laboratoire d'Océanographie et du Climat: Expérimentation et Approches Numériques, Institut Pierre Simon Laplace, Université Pierre et Marie Curie, Paris, France.
[2]Laboratoire de Météorologie Dynamique, Institut Pierre Simon Laplace, Ecole Normale Supérieure, Paris, France.

0094-8276/12/2012GL051294

convection [*Liebmann and Smith*, 1996]. We also consider the zonal wind at 850 hPa (U850) provided by the ERA-Interim program [*Dee et al.*, 2011]. The perturbation pattern of each MJO event is extracted using the LMA technique described by *Goulet and Duvel* [2000] and by *Duvel and Vialard* [2007]. Here we only give a brief account of the main features of this technique. The input signal is a time series filtered to remove interannual and seasonal fluctuations. This filtering is done by removing all harmonics corresponding to periods larger than 120 days. The result is a time series $S_x(t)$, where x is a grid point ($1 \leq x \leq X$) and t is the time step in day ($1 \leq t \leq T$). The LMA is based on *a series* of complex EOF (CEOF) computed on relatively small time sections of $S_x(t)$. Here, the time section is 120-day long and the lag between two analyses is 5 days. In addition, a Welch window is applied to avoid end effects and to maximize the signal at the center of the time-section. Every 5 days, this defines a time series of 120 days $s_x^t(i)$ with i varying in [t − 59, t + 60], where t is the time at the center of the time section. A CEOF is thus performed for each time series $s_x^t(i)$.

[6] The cross-spectrum matrix is computed only for the five first harmonics (corresponding to periods between 24 and 120 days). The first eigenvector of this 5 × 5 matrix, associated with a percentage of variance π_t, is the normalized complex temporal spectrum $\psi_t(k)$ that, by definition, best characterize the intraseasonal fluctuation for the considered time section centered on t. The percentage of variance π_t represents the degree of spatial organization of this fluctuation. A maximum value of π_t represents a time section for which the intraseasonal perturbation is locally (in time) better organized at planetary-scale that for the adjacent time sections (i.e., t − 5d and t + 5d). We thus consider only the maxima in the π_t time series that define an ensemble of M intraseasonal events. For each event m ($1 \leq m \leq M$), the normalized complex spectrum $\psi_m(k)$ is used to compute the corresponding complex spatial pattern $Z_m(x)$ that gives maps of amplitude and relative phase; the relative phase represents the propagative properties. The strength of the LMA is that the π_m are large, simply because the time-section is small. This means that the spectral key $\psi_m(k)$ and the spatial patterns $Z_m(x)$ well *represent the actual perturbation* in the center of the time section m. The LMA gives a simple mathematical formulation for the perturbation pattern associated with each intraseasonal event. For the 1979–2010 period, we identify M = 60 MJO events with a time window centered between December and March. For each event, the *MJO amplitude* for a given region (x) and a given event (m) is defined as the modulus of the complex pattern element $Z_m(x)$.

[7] We will also compare our result to the MJO variability deduced from the widely used RMM (Real-time Multivariate MJO) indexes developed by *Wheeler and Hendon* [2004, hereinafter WH]. These indexes are based on the projection of equatorial (15°S to 15°N average) anomalies of OLR and zonal wind at 850 hPa and 200 hPa, onto a couple of equatorial EOFs. The extracted MJO amplitude and phase are thus relative to a unique or *canonical MJO structure* given by these two EOFs. It is important to underline that, while it covers all longitudes, the WH index gives an *instantaneous* (i.e., for a given day) magnitude and a longitudinal phase for an equivalent canonical MJO perturbation. On the contrary, the LMA gives the amplitude and the actual spatial pattern (for one or several parameters) for the *entire duration of a given MJO event.* In order to compare our results to the WH approach, we thus compute an average WH amplitude index for ±20 days around the center of the time section m (note that averaging for ±30 does not significantly change the conclusion).

3. The MJO Amplitude and Its Variability

[8] For the OLR, the average MJO amplitude field over the 60 boreal winter MJO events is maximal on a zonal band around 10°S and between 60°E and 200°E (Figure 1a). As noticed by previous studies [e.g., *Bellenger and Duvel*, 2007] the MJO amplitude is maximal over ocean regions and minimal over the large islands of the Maritime Continent. The reduced perturbations over land regions may partly explain the amplitude gap south of Java (between IO and MC) and south of Papua New Guinea (between MC and PO). The largest OLR and U850 amplitude is found over ocean regions south of the Maritime Continent and north of Australia (MC). The preeminence of this narrow band of ocean is somewhat surprising since it is surrounded by islands and continental regions for which the intraseasonal variability is reduced. The two other basins of large OLR perturbation are the IO and the PO ocean basins.

[9] As for the OLR, the U850 perturbation is maximal on a zonal band around 10°S and between 60°E and 200°E (Figure 1a). Over MC, the maximum U850 MJO amplitude is obtained over ocean regions south of the Maritime Continent and north of Australia, showing the close relation between convective and low-level wind perturbations. An intriguing result is the larger U850 perturbation over PO compared to IO, whereas the opposite is observed for the OLR. This may be explained considering the Gill-Type dynamical response to a basin-scale convective heating close to the Equator [*Gill*, 1980]. This type of dynamical response gives easterly wind to the east and westerly wind under and to the west of the convective perturbation. There is no large convective perturbation west of IO and thus weak easterly wind perturbation over IO. Over PO, easterly wind perturbation is expected when the convection is maximal over MC and may explain the larger U850 MJO amplitude.

[10] The present study focuses on the *event-to-event variability of the MJO structure.* One may expect that this variability is maximal where the average MJO amplitude (Figure 1a) is large. However, this is not obvious since the event-to-event variability can be small for regions where the MJO characteristic is relatively reproducible. The event-to-event standard deviation of the MJO amplitude among the 60 events (Figure 1b) is indeed maximal over the 3 basins. However, for both OLR and U850, the event-to-event variability of the MJO amplitude is larger over PO while this amplitude is maximal over MC (Figure 1a). For both OLR and wind, the event-to-event variability is smaller over IO.

[11] The average or planetary-scale MJO amplitude A_{TOT} is defined as the amplitude spatially averaged over the three basins (with basin average amplitude noted A_{IO}, A_{MC}, A_{PO}). A_{TOT} varies typically between 10 and 25 Wm^{-2} for the OLR and between 1 and 3.5 ms-1 for U850 (Figure 1c). There is generally a good agreement between the average amplitude A_{TOT} for both parameters (correlation of 0.85), showing the close relationship between the convective activity and the low-level wind perturbation at the planetary-scale. For both

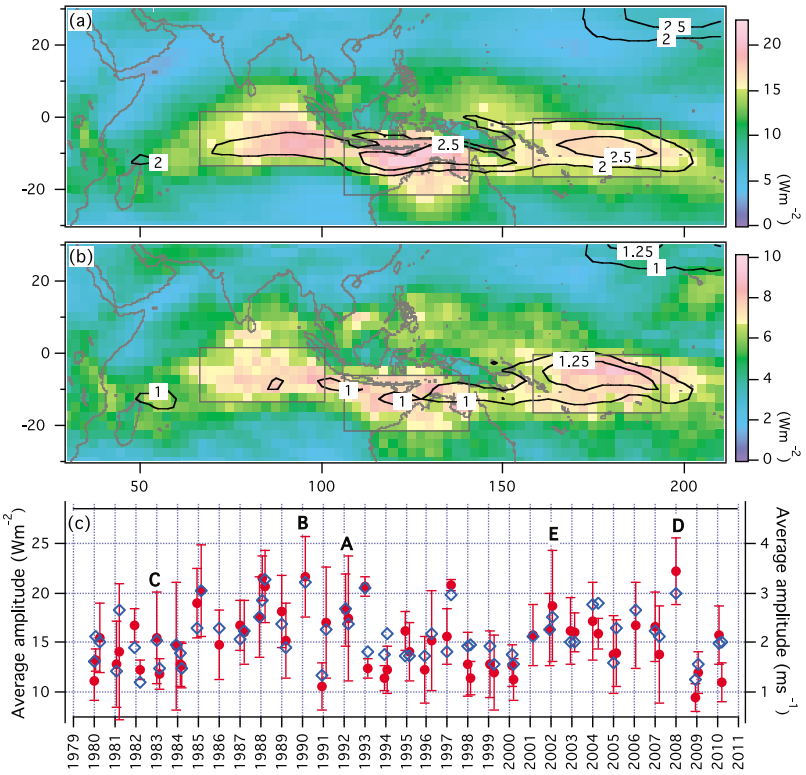

Figure 1. Statistics on the 60 boreal winter MJO events extracted by the LMA from the NOAA OLR dataset (DJFM 1979–2010) for the OLR (Wm^{-2}, colors) and the zonal wind at 850 hPa (U850, ms^{-1}, contours): (a) average MJO amplitude; (b) event-to-event standard deviation of the MJO amplitude among the 60 events. IO, MC and PO regions are superimposed. (c) Average OLR amplitude (circles), average U850 amplitude (diamonds) and standard deviation of OLR amplitudes (V_{TOT}, sticks) among the 3 basins (IO, MC and PO).

OLR and U850, one may notice some decadal variability of A_{TOT} (Figure 1c), with almost no events with A_{TOT} < 15 Wm^{-2} (<2 ms^{-1}) between 1985 and 1990 and between 2001 and 2008 for the OLR. Between 1993 and 2000, most events have A_{TOT} < 15 Wm^{-2} (<2 ms^{-1}) and there is no event with A_{TOT} > 20 Wm^{-2} (>3 ms^{-1}), with the noticeable exception of March 1997 event at the origin of the strong El Niño of 1998. This interannual variability of A_{TOT} is related neither to ENSO (near 0 correlation coefficient with the Niño 3.4 index) nor to the Pacific Decadal Oscillation [*Mantua and Hare*, 2002] (0.12 correlation coefficient). The source of this interannual and decadal variability remains unclear.

[12] The longitudinal inhomogeneity V_{TOT} is defined as the rms of the deviation of the amplitude of the three basins

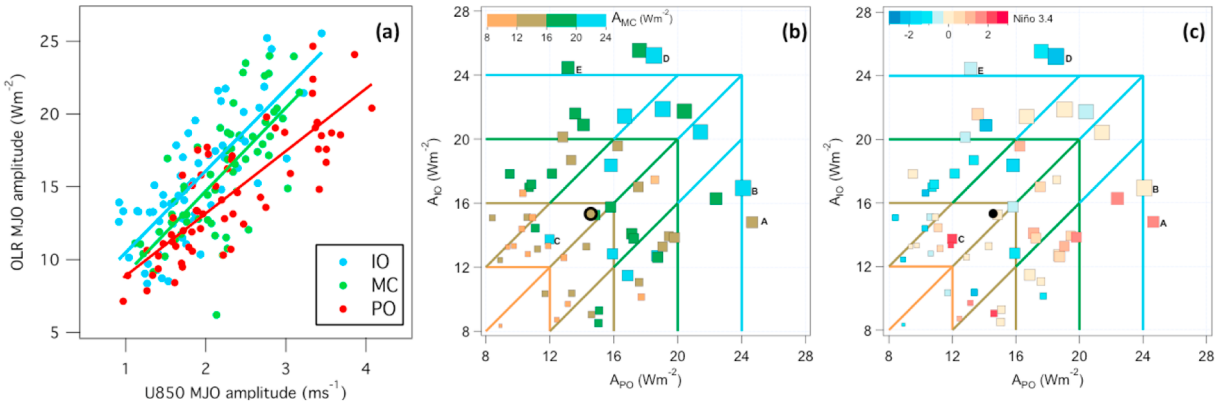

Figure 2. (a) Scatterplots of amplitudes of OLR and U850 over each basin (defined in Figure 1) for each MJO event. Best linear fits are plotted. Distribution of the MJO events amplitude (Wm^{-2}) of the OLR perturbations averaged over the IO basin (A_{IO}, Y-axis) and PO basin (A_{PO}, X-axis). (b) The square size and color represent the average amplitude over MC basin. (c) Same as Figure 2b but the color represents the Niño 3.4 index. The disk represents the all events average MJO amplitudes. Colored lines represent Y = X(±4) and the upper limits of the A_{MC} color scale categories to ease the comparison between A_{IO}, A_{MC} and A_{PO}.

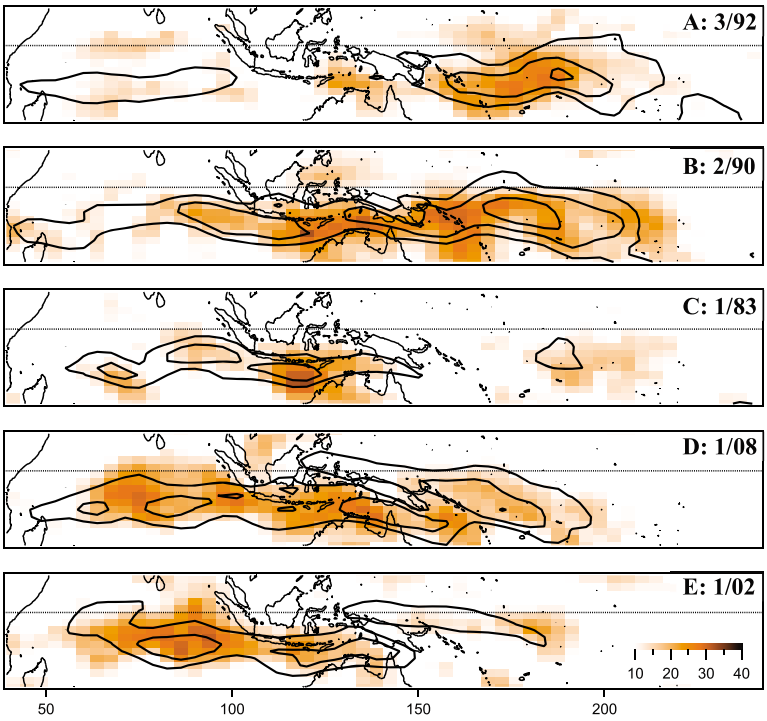

Figure 3. Amplitude of perturbation of OLR (color, Wm^{-2}) and U850 (contours, every 1 ms^{-1} from 2 ms^{-1}) for five single MJO events.

from A_{TOT}. For the OLR, some events have relatively uniform amplitude (small V_{TOT}) among the three basins, such as the event of January 1993 that corresponds to the TOGA-COARE event [*Yanai et al.*, 2000]. Some events, such as event E (January 2002), have large V_{TOT} suggesting a concentration of the OLR perturbation over one or two basins. This is also suggested by the low correlation between each pair of basins considering the MJO amplitude time series of the 60 events: 0.43 for IO-MC; 0.37 for MC-PO and; 0.18 for IO-PO.

[13] In addition, the close relationship between convective and low-level wind perturbation at the planetary-scale also holds at the basin-scale. OLR and U850 perturbations amplitudes are indeed linearly related over each basin (Figure 2a) with correlation coefficients of 0.77, 0.71 and 0.83 for IO, MC and PO respectively. This relation however slightly changes from one basin to another with U850 perturbations stronger over PO for a similar convective perturbation due to the planetary-scale dynamical response even for a local convective heating perturbation.

4. The MJO Pattern Variability

[14] Figure 2 presents a concise picture of the MJO amplitude distribution over the 3 basins. OLR and U850 perturbations are well correlated over each basin (Figure 2a). The position of a given event relative to the diagonal ($A_{IO} = A_{MC=}A_{PO}$, Figure 2b) may thus be interpreted as a deformation of the MJO patterns (for OLR and U850) relative to a "canonical" MJO represented by identical amplitude for the 3 basins. Indeed, the average MJO amplitude for each basin (the circle of Figure 2b) is quite uniform and around 15 Wm^{-2}. The MJO amplitude of the three basins tends to be located along the diagonal ($A_{IO} = A_{MC=}A_{PO}$), indicating a tendency for a general growth of the MJO amplitude for all longitudes. However, there is also a relatively large scatter of the MJO amplitude distribution (as already depicted by the error bar in Figure 1c). This amplitude can be almost twice as large over one basin compared to the others (e.g., events A or E giving a large standard deviation in Figure 1c).

[15] In order to illustrate this diversity, OLR and U850 amplitude patterns are shown in Figure 3 for five "extreme" MJO events having large amplitude differences for the 3 basins (ABCDE in Figure 1c and in Figure 2b). Event A (March 1992) is an MJO perturbation confined over the Pacific Ocean. Event B (February 1990) has amplitude distributed over PO and MC, but is rather weak over IO. According to LMA results, this event B is one of the strongest and best-organized intraseasonal perturbations of the whole existing OLR series. Event C (January 1983) is confined over the MC basin, showing that EL Niño conditions do not systematically correspond to an eastward extension of the MJO. Event D (January 2008) is a strong event mostly distributed over IO and MC. Event E (January 2002) is particularly strong and confined over the Indian Ocean. Such an event confined over IO is certainly comparable to Indian Ocean MJO type of *Jones et al.* [2004]. Figure 3 shows that events with large standard deviation between the 3 basins may be due to a concentration over a single basin (A, C and E) or over two basins (B and D). A noteworthy feature is the generally good agreement between convective and wind perturbation patterns. For example, both OLR and U850 perturbations are concentrated over PO for event A and over IO for event E.

[16] The MJO amplitude tends to be stronger over PO for El Niño conditions and over IO for La Niña conditions

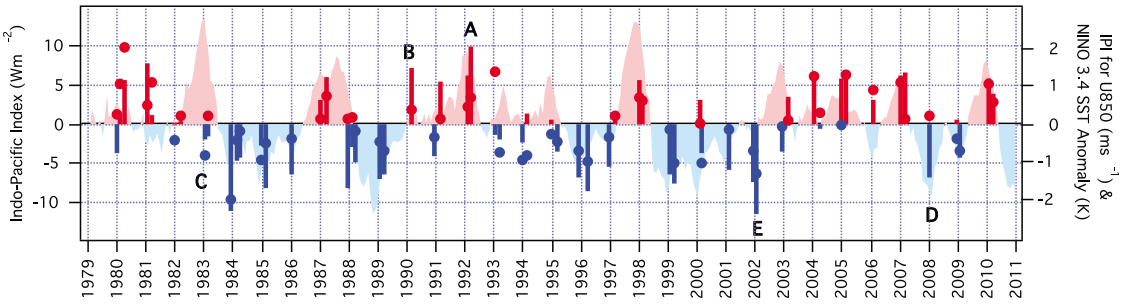

Figure 4. MJO Indo-Pacific Index (IPI) for each boreal winter MJO events (bars). The IPI (IPI_{U850}, circles) is defined as the difference in amplitude of the MJO OLR (U850) perturbation between PO and IO. Because U850 amplitudes are stronger over PO, IPI_{U850} is centered by subtracting its average value (0.46 ms^{-1}). The Niño 3.4 index is superimposed.

(Figure 2c). However, there is no systematic relation, and the MJO amplitude over PO can be either small (e.g., event C) or large (event A) for El Niño conditions. The relation between the MJO pattern and ENSO is clearer by considering large PO amplitude is regard to IO. Most events on the right side of the $A_{PO} = A_{IO} - 4$ line (Figure 2c) for El Niño conditions. Reciprocally, most MJO events on the left side of the $A_{IO} = A_{PO} + 4$ line correspond to La Niña conditions. This fact suggests an Indo-Pacific *alternation* of the MJO amplitude related to ENSO, rather than an *eastward extension* of the MJO signal for El Niño condition, as described by *Kessler* [2001]. Note that this East-West alternation also appears to be the primary variability of the MJO pattern from an EOF analysis among the 60 OLR amplitude fields (see auxiliary material).[1] Based on this results, we define an Indo-Pacific Index based on the MJO amplitude for the OLR, $IPI = A_{PO} - A_{IO}$, expecting positive IPI for El Niño conditions and negative IPI in La Niña conditions. It is also possible to construct an IPI for U850 (IPI_{U850}). Because U850 perturbations are stronger over PO, the average IPI_{U850} is subtracted. IPI_{U850} is well related to IPI (correlation of 0.7, Figure 4), showing the tendency of the low-level wind perturbation to be stronger on the basin where the convective perturbation is stronger.

[17] The MJO IPI has a strong interannual and decadal variations (Figure 4). It is particularly interesting to note that both sign and magnitude of the index tend to be homogeneous for a given year. This suggests that the longitudinal distribution of the amplitude is forced by some interannual variability. This interannual variability is mostly but not exclusively linked to ENSO, as demonstrated by neutral ($IPI \approx 0$) MJO events during winter 1982–83 or by events with negative IPI during the neutral ENSO years 1988–89 or 2001–02. Indeed, the link between the IPI and the Niño3.4 index is obvious in Figure 4 but their actual linear correlation coefficient is only 0.47. This suggests that other forcings are also influencing the IPI, such as the Dipole Mode Index [*Saji et al.*, 1999] or the Pacific Decadal Oscillation [*Mantua and Hare*, 2002]. However, no evident relations were found with these different indexes.

5. Relation With the WH Index

[18] The WH index is widely used to depict the day-to-day variability of the MJO phase and amplitude in real time. This index is useful to assess operational MJO forecasts [*Gottschalck et al.*, 2010], or, for example, to construct composites in regard to different MJO phases. During an MJO event, as defined here, the WH index may have variable amplitudes for the different MJO phases. In order to compare the planetary-scale amplitude obtained here (i.e., the A_{TOT}) to the WH amplitude, we simply compute average WH amplitude for ±20 days around the central day of each of our 60 MJO events (different time intervals give comparable results up to ±30 days). The linear correlation coefficient between this average WH amplitude (that takes into account OLR, U850 and U at 200 hPa) and A_{TOT} is 0.74 for U850 and 0.63 for the OLR, showing the good correspondence between the two approaches for both parameters (Figure 5). The main cause of discrepancy is certainly due to the fact that the WH index is a projection over a unique *canonical MJO pattern*, while an LMA event may have any spatial pattern. The scattering in Figure 5 is thus also a measure of the difference between the pattern of the MJO events and the canonical MJO pattern. More detailed

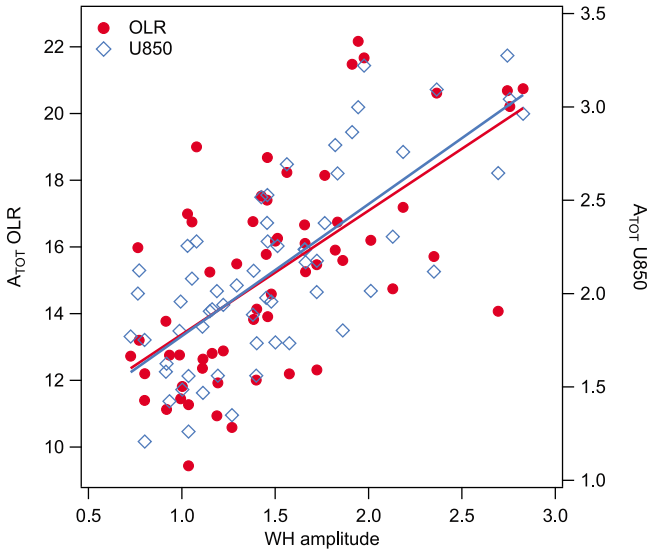

Figure 5. Scatterplots of the average MJO amplitude over the 3 basins (A_{TOT}) of the OLR (red circles) and U850 (open blue squares) as a function of the average WH amplitude index for ±20 days around the center of the LMA-extracted MJO event. The corresponding best linear fits are also plotted.

[1]Auxiliary materials are available in the HTML. doi:10.1029/2012GL051294.

comparison between the two approaches is very interesting but is beyond the scope of this study.

6. Summary and Discussion

[19] We study the event-to-event variability of the MJO patterns for the OLR and the low-level zonal wind during the boreal winter season between 1979–2010. For this period, the LMA detects and characterizes 60 MJO events. On the average, OLR and U850 MJO perturbations are maximal over three basins (IO, MC and PO). The event-to-event variability of the amplitude is also concentrated over the three basins, with maximum values over PO. Planetary-scale MJO amplitude is defined as the average amplitude over the three basins. This planetary-scale amplitude exhibits similar decadal variability for both OLR and U850. A careful examination of the event-to-event variability also reveals differences in the MJO pattern with different distribution of the amplitude over the 3 basins. Some extreme MJO events have large amplitude over one basin only. The low-level wind perturbations pattern is generally linked to convective perturbations with maximum U850 perturbation on the same basin as for the OLR.

[20] The primary variability of the MJO pattern is an alternation between events having maximum amplitude on IO or on PO. This alternation is measured here by an Indo-Pacific Index (IPI) that is well related to the Niño3.4 index. This shows that the impact of ENSO on the MJO is not only an extension of the perturbation further east [*Kessler*, 2001], but also an increase of the MJO perturbation over the western Pacific and a diminution of the MJO perturbation over the eastern Indian Ocean. However, this MJO alternation is not related only to ENSO and some groups of MJO events for a given winter may have an IPI not related to the Niño3.4 index. This is the case for winter 82–83 with a neutral IPI for large Niño3.4 index, or for winter 89–90 with a large IPI associated to a neutral Niño3.4 index. Our results are not in agreement with *Jones et al.* [2004] who found no significant differences between MJO events occurring in different phase of ENSO. As by *Jones and Carvalho* [2006] we find however a low frequency variability of the MJO amplitude, even if there is no evident variation in the number of MJO events.

[21] There is certainly a common physical origin for MJO events concentrated over a single basin and for canonical MJO events propagating over the three basins with comparable amplitude. The existence of some strong intraseasonal perturbations confined over the Pacific, with weak perturbation over the Indian Ocean, shows that the Indian Ocean is not the only source region of the MJO [see also *Matthews*, 2008]. In addition, there is no clear indication of a forcing by equatorial waves coming from the west. Indeed, the wind perturbation tends rather to be confined in the region of maximum OLR perturbation (Figures 1a and 3), as expected for a dynamical response to convective heating. The central question for the boreal winter MJO could thus be to know the mechanism responsible for the triggering over one of the three basins and for the eventual propagation of the perturbation over the basin located eastward. The research of different environments determining the MJO amplitude or particular MJO patterns is however not straightforward because non-linear effects of the MJO perturbation can modify the mean state, in particular the circulation [*Bellenger et al.*, 2009] or the SST [e.g., *Duvel*, 2012]. The direction of causality is thus not evident, even for the ENSO phase, since the MJO may impact the phase of El Niño triggering or retreat. In summary, we find a decadal variability of the average MJO amplitude with no relation with ENSO and an Indo-Pacific alternation of the amplitude mostly, but not uniquely, related to ENSO. The physical source of this inter-event variability in MJO amplitude and pattern remains to be investigated.

[22] **Acknowledgments.** The authors thank the anonymous reviewers for their useful comments. Hugo Bellenger was partly funded by the Agence Nationale pour la Recherche, project ANR-10-Blanc-616 METRO, and the European Union Seventh Framework Programme EUCLIPSE project under grant agreement n 244067.

[23] The Editor thanks the anonymous reviewer for assisting with the evaluation of this paper.

References

Bellenger, H., and J. P. Duvel (2007), Intraseasonal perturbations related to the seasonal march of the Indo-Pacific monsoons, *J. Clim.*, *20*, 2853–2863, doi:10.1175/JCLI4182.1.

Bellenger, H., J. P. Duvel, M. Lengaigne, and P. Le Van (2009), Impact of organized intraseasonal convective perturbations on the tropical circulation, *Geophys. Res. Lett.*, *36*, L16703, doi:10.1029/2009GL039584.

Dee, D. P., et al. (2011), The ERA-Interim reanalysis: Configuration and performance of the data assimilation system, *Q. J. R. Meteorol. Soc.*, *137*, 553–597, doi:10.1002/qj.828.

Duvel, J. P. (2012), Oceans and air-sea interaction, in *Intraseasonal Variability of the Atmosphere–Ocean Climate System*, edited by W. K. M. Lau and D. E. Waliser, pp. 513–536, Springer, Berlin.

Duvel, J. P., and J. Vialard (2007), Indo-Pacific sea surface temperature perturbations associated with intraseasonal oscillation of the tropical convection, *J. Clim.*, *20*, 3056–3082, doi:10.1175/JCLI4144.1.

Duvel, J. P., H. Bellenger, G. Bellon, and M. Remaud (2012), An event-by-event assessment of tropical intraseasonal perturbations for general circulation models, *Clim. Dyn.*, doi:10.1007/s00382-012-1303-6, in press.

Gill, A. E. (1980), Some simple solutions for heat-induced tropical circulation, *Q. J. R. Meteorol. Soc.*, *106*, 447–462, doi:10.1002/qj.49710644905.

Gottschalck, J., et al. (2010), A framework for assessing operational Madden–Julian Oscillation forecasts: A CLIVAR MJO Working Group project, *Bull. Am. Meteorol. Soc.*, *91*, 1247–1258, doi:10.1175/2010BAMS2816.1.

Goulet, L., and J. P. Duvel (2000), A new approach to detect and characterize intermittent atmospheric oscillations: Application to the intraseasonal oscillation, *J. Atmos. Sci.*, *57*, 2397–2416, doi:10.1175/1520-0469(2000)057<2397:ANATDA>2.0.CO;2.

Jones, C., and L. M. V. Carvalho (2006), Changes in the activity of the Madden-Julian Oscillation during 1958–2004, *J. Clim.*, *19*, 6353–6370, doi:10.1175/JCLI3972.1.

Jones, C., L. M. V. Carvalho, R. W. Higgins, D. E. Waliser, and J. K. E. Schemm (2004), Climatology of tropical intraseasonal convective anomalies: 1979–2002, *J. Clim.*, *17*, 523–539, doi:10.1175/1520-0442(2004)017<0523:COTICA>2.0.CO;2.

Kessler, W. S. (2001), EOF representation of the Madden–Julian Oscillation and its connection with ENSO, *J. Clim.*, *14*, 3055–3061, doi:10.1175/1520-0442(2001)014<3055:EROTMJ>2.0.CO;2.

Liebmann, B., and C. A. Smith (1996), Description of a complete (interpolated) outgoing longwave radiation dataset, *Bull. Am. Meteorol. Soc.*, *77*, 1275–1277.

Mantua, N. J., and S. R. Hare (2002), The Pacific Decadal Oscillation, *J. Oceanogr.*, *58*, 35–44, doi:10.1023/A:1015820616384.

Matthews, A. J. (2008), Primary and successive events in the Madden-Julian Oscillation, *Q. J. R. Meteorol. Soc.*, *134*, 439–453, doi:10.1002/qj.224.

Saji, N. H., B. N. Goswami, P. N. Vinayachandran, and T. Yamagata (1999), A dipole mode in the tropical Indian Ocean, *Nature*, *401*, 360–363, doi:10.1038/43854.

Wheeler, M., and H. H. Hendon (2004), An all-season real-time multivariate MJO index: Development of an index for monitoring and prediction, *Mon. Weather Rev.*, *132*, 1917–1932, doi:10.1175/1520-0493(2004)132<1917:AARMMI>2.0.CO;2.

Xavier, P. K., J. P. Duvel, P. Braconnot, and F. J. Doblas-Reyes (2010), An evaluation metric for intraseasonal variability in climate models, *J. Clim.*, *23*, 3497–3508, doi:10.1175/2010JCLI3260.1.

Yanai, M., B. Chen, and W. W. Tung (2000), The Madden–Julian Oscillation observed during the TOGA COARE IOP: Global view, *J. Atmos. Sci.*, *57*, 2374–2396, doi:10.1175/1520-0469(2000)057<2374:TMJOOD>2.0.CO;2.

Yano, J. I., R. Blender, C. Zhang, and K. Fraedrich (2004), 1/f noise and pulse-like events in the tropical atmospheric surface variabilities, *Q. J. R. Meteorol. Soc.*, *130*, 1697–1721, doi:10.1256/qj.03.42.

Zhang, C. (2005), Madden-Julian Oscillation, *Rev. Geophys.*, *43*, RG2003, doi:10.1029/2004RG000158.

H. Bellenger, Laboratoire d'Océanographie et du Climat: Expérimentation et Approches Numériques, Institut Pierre Simon Laplace, Université Pierre et Marie Curie, 4 place Jussieu, F-75005 Paris CEDEX, France. (hugo.bellenger@locean-ipsl.upmc.fr)

J. P. Duvel, Laboratoire de Météorologie Dynamique, Institut Pierre Simon Laplace, Ecole Normale Supérieure, 24 rue Lhomond, F-75231 Paris CEDEX, France.